Influence of Thermal Radiation on the Unsteady Mixed Convection Flow of a Jeffrey Fluid over a Stretching Sheet

Tasawar Hayat[a,b] and Meraj Mustafa[a]

[a] Department of Mathematics, Quaid-I-Azam University 45320, Islamabad 44000, Pakistan
[b] Department of Mathematics, College of Science, King Saud University, P.O. Box 2455, Riyadh 11451, Saudi Arabia

Reprint requests to T. H.; E-mail: pensy_t@yahoo.com

Z. Naturforsch. **65a,** 711 – 719 (2010); received August 26, 2009 / revised November 21, 2009

This study is concerned with the effect of thermal radiation on the unsteady mixed convection flow of a Jeffrey fluid past a porous vertical stretching surface. The arising problems of flow and heat transfer are solved analytically by employing homotopy analysis method (HAM). It is observed that the flow field is influenced appreciably by the unsteadiness parameter ζ, suction parameter S, mixed convection parameter λ, Deborah number β, Prandtl number Pr, and the radiation parameter Nr. Our performed computations depict that the heat transfer rate is increased with increasing values of Pr, Nr, and ζ.

Key words: Series Solution; Jeffrey Fluid; Heat Transfer.

1. Introduction

The flows of non-Newtonian fluids [1 – 10] have gained importance because of their extensive applications in industry and technology. The boundary layer flows of non-Newtonian fluids over a stretching surface along with heat transfer characteristics are also of great importance in engineering. Such flows have been studied widely in the last few years. Examples of such flows include hot rolling, wire drawing, crystal growing, extrusion of sheets etc. Crane [11] considered the flow of a viscous a fluid over a linear stretching surface. Subsequently, various stretching flow problems along with heat transfer have been considered in many investigations [12 – 20]. Much attention in the past has been given to the two-dimensional stretching flow problems. Little effort is devoted to examine the time-dependent stretching flow problems [21 – 25].

In many practical situations the surface stretches in a quiescent fluid. The fluid flow is caused by motion of a solid surface and by thermal buoyancy. The flow and heat transfer are therefore determined by surface motion and buoyancy. It is obvious that buoyancy forces arise from the heating or cooling of continuous stretching sheets. These forces alter the flow and thermal fields and thereby the heat transfer characteristics of the manufacturing processes. The influence of thermal buoyancy on heat transfer from a continuous moving surface in viscous and incompressible fluids is analyzed in the studies [26 – 30]. Elbashbeshy and Bazid [24] presented an exact similarity solution for unsteady momentum and heat transfer flow over a linear stretching surface. Very recently, Mukhopadhyay [25] examined the effect of thermal radiation on unsteady mixed convection flow and heat transfer over a porous stretching surface in a porous medium. The purpose of the present investigation is to analyze the heat transfer over an unsteady mixed convection flow of a Jeffrey fluid over a stretched vertical surface. Series solution of the problem is obtained by employing the homotopy analysis method (HAM) [31 – 45]. This method is a very powerful analytical tool and has been already applied by several investigators to various problems. Graphical results for interesting parameters are presented. Numerical results of skin friction coefficient and local Nusselt number are tabulated for various values of the embedding parameters.

2. Mathematical Formulations

We consider heat transfer analysis in a Jeffrey fluid. The flow and heat transfer characteristics are due to stretching of a heated or cooled vertical surface with velocity $u_w = \frac{cx}{1-\alpha t}$ and temperature distribution $T_w = T_\infty + 1/2 T_0 Re_x x^{-1}(1-\alpha t)^{-1} = T_\infty + T_0 \frac{cx}{2\nu}(1-\alpha t)^{-2}$, where $Re_x = \frac{u_w x}{\nu}$ is the local Reynolds number. The

0932–0784 / 10 / 0800–0711 $ 06.00

density variation and the buoyancy effects are taken into account and the Boussinesq approximation for both the temperature and concentration gradient is adopted. The fluid is electrically conducting in the presence of applied magnetic field B_0. The boundary layer equations in the absence of heat generation and viscous dissipation are

$$\frac{\partial u}{\partial x}+\frac{\partial v}{\partial y}=0, \tag{1}$$

$$\begin{aligned}&\frac{\partial u}{\partial t}+u\frac{\partial u}{\partial x}+v\frac{\partial u}{\partial y}\\&=\frac{\nu}{1+\lambda_1}\left[\frac{\partial^2 u}{\partial y^2}+\lambda_2\left(\frac{\partial^3 u}{\partial y^2\partial t}+u\frac{\partial^3 u}{\partial y^2\partial x}\right.\right.\\&\qquad\left.\left.+\frac{\partial u}{\partial x}\frac{\partial^2 u}{\partial y^2}+3\frac{\partial u}{\partial y}\frac{\partial^2 u}{\partial x\partial y}+v\frac{\partial^3 u}{\partial y^3}\right)\right]\\&\quad+g\beta_{\mathrm{T}}(T-T_\infty)-\frac{\sigma}{\rho}B_0^2(t)u,\end{aligned} \tag{2}$$

$$\frac{\partial T}{\partial t}+u\frac{\partial T}{\partial x}+v\frac{\partial T}{\partial y}=\frac{k}{\rho C_{\mathrm{p}}}\frac{\partial^2 T}{\partial y^2}-\frac{1}{C_{\mathrm{p}}}\frac{\partial q_r}{\partial y}. \tag{3}$$

The subjected boundary conditions are

$$\begin{aligned}&u=U_{\mathrm{w}}(x)=\frac{cx}{1-\alpha t},\quad v=v_{\mathrm{w}}=-\frac{v_0}{(1-\alpha t)^{1/2}},\\&T=T_{\mathrm{w}},\quad \text{at } y=0,\\&u\to 0,\quad \frac{\partial u}{\partial y}\to 0,\quad T\to T_\infty \quad \text{as } y\to\infty,\end{aligned} \tag{4}$$

where $\alpha t<1$, x and y are the Cartesian coordinates, ν is the kinematic viscosity, t is the time, u and v are the velocity components along x- and y-axes, respectively, λ_2 is the relaxation time, and λ_1 is the ratio of relaxation to the retardation time, T is the fluid temperature, g is the gravitational acceleration, β_{T} is the volumetric coefficient of thermal expansion, k is the coefficient of thermal expansion, q_{r} is the radiative heat flux and C_{p} is the specific heat.

Incorporating the Roseland approximation we obtain $q_{\mathrm{r}}=-\frac{4\sigma}{3k^*}\frac{\partial T^4}{\partial y}$, where σ is the Stefan-Boltzman constant and k^* is the absorption coefficient. We assume that the temperature difference within the flow is such that T^4 may be expanded in a Taylor series. Expanding T^4 about T_∞ and neglecting higher orders we get, $T^4=4T_\infty^3T-3T_\infty^4$. Now (3) becomes

$$\frac{\partial T}{\partial t}+u\frac{\partial T}{\partial x}+v\frac{\partial T}{\partial y}=\left(\frac{k}{\rho C_{\mathrm{p}}}+\frac{16\sigma T_\infty^3}{3\rho C_{\mathrm{p}}k^*}\right)\frac{\partial^2 T}{\partial y^2}. \tag{5}$$

Introducing

$$\begin{aligned}&\psi=x\sqrt{\frac{c\nu}{1-\alpha t}}f(n),\quad \theta(\eta)=\frac{T-T_\infty}{T_{\mathrm{w}}-T_\infty},\\&\eta=\sqrt{\frac{c}{\nu}}\Gamma(1-\alpha t)^{-1/2},\end{aligned} \tag{6}$$

inserting into (2)–(5), we have

$$\begin{aligned}&f'''+(1+\lambda_1)\left(ff''-f'^2-\zeta\left(\frac{\eta}{2}f''+f'\right)\right.\\&\quad\left.+\lambda\theta-M^2f'\right)+\beta\left(\zeta\left(\frac{\eta}{2}f^{iv}+2f'''\right)\right.\\&\quad\left.+2f'f'''+3f''^2-ff^{iv}\right)=0,\end{aligned} \tag{7}$$

$$\frac{1}{Pr}\left(1+\frac{4}{3Nr}\right)\theta''+f\theta'-\theta f'-\frac{\zeta}{2}(\eta\theta'+4\theta)=0, \tag{8}$$

$$\begin{aligned}&f(0)=S,\quad f'(0)=1,\quad \theta(0)=1,\\&f'(\infty)\to 0,\quad f''(\infty)\to 0,\quad \theta(\infty)\to 0,\end{aligned} \tag{9}$$

where $Pr=\mu C_{\mathrm{p}}/k$ is the Prandtl number, μ is the dynamic viscosity, λ is the dimensionless mixed convection parameter, ζ is the unsteadiness parameter, Nr is the radiation parameter, and β is the dimensionless material parameter known as Deborah number. These are given by

$$\begin{aligned}&\lambda=\frac{g\beta_{\mathrm{T}}(T_{\mathrm{w}}-T_\infty)x^3/\nu^2}{u_{\mathrm{w}}^2x^2/\nu^2}=\frac{Gr_x}{Re^2},\\&\zeta=\frac{\alpha}{c},\quad Nr=\frac{KK^*}{4\sigma^*T_\infty^3},\quad \beta=\frac{\lambda_2 c}{1-\alpha t},\end{aligned} \tag{10}$$

with $Gr_x=g\beta_{\mathrm{T}}(T_{\mathrm{w}}-T_\infty)x^3/\nu^2$ being the local Grashof number and $Re_x=u_{\mathrm{w}}x/\nu$ is the local Reynolds number. It is noticed that $\lambda>0$ corresponds to an assisting flow (heated plate), $\lambda<0$ corresponds to an opposing flow (cooled plate), and $\lambda=0$ yields forced convection flow.

The skin friction coefficient and the local Nusselt number Nu_x are given by

$$C_{\mathrm{f}}=\frac{\tau_{\mathrm{w}}}{\rho U_{\mathrm{w}}^2},\quad Nu_x=\frac{xq_{\mathrm{w}}}{k(T_{\mathrm{w}}-T_\infty)}, \tag{11}$$

in which τ_{w} and q_{w} are the wall skin friction and the wall heat flux, respectively, which are defined by the

following expressions:

$$\tau_{\mathrm{w}} = \frac{\mu}{1+\lambda_1}\left[\frac{\partial u}{\partial y} + \lambda_2\left(\frac{\partial^2 u}{\partial y \partial t} + u\frac{\partial^2 u}{\partial y \partial x} + 2\frac{\partial u}{\partial x}\frac{\partial u}{\partial y} + v\frac{\partial^2 u}{\partial y^2}\right)\right]_{y=0}, \quad (12)$$

$$q_{\mathrm{w}} = -k\left(\frac{\partial T}{\partial y}\right)_{y=0}.$$

The dimensionless forms of above expressions are

$$Re_x^{1/2} C_{\mathrm{f}} = \frac{1}{1+\lambda_1}\left[f'' + \beta\left\{\zeta\left(f'''\frac{\eta}{2} + \frac{3}{2}f''\right) + 3f'f'' - ff'''\right\}\right]_{\eta=0}, \quad (13)$$

$$Nu_x/Re_x^{1/2} = -\theta'(0).$$

3. Homotopy Analysis Solutions

The velocity $f(\eta)$ and the temperature $\theta(\eta)$ in terms of the set of base functions

$$\{\eta^k \exp(-n\eta) | k \geq 0, n \geq 0\}$$

can be written as

$$f(\eta) = a_{0,0}^0 + \sum_{n=0}^{\infty}\sum_{k=0}^{\infty} a_{m,n}^k \eta^k \exp(-n\eta), \quad (14)$$

$$\theta(\eta) = \sum_{n=0}^{\infty}\sum_{k=0}^{\infty} b_{m,n}^k \eta^k \exp(-n\eta), \quad (15)$$

in which $a_{m,n}^k$ and $b_{m,n}^k$ are the coefficients. By the rule of solution expressions and the boundary conditions (10), the initial guesses f_0 and θ_0 of $f(\eta)$ and $\theta(\eta)$ are chosen as

$$f_0(\eta) = S + 1 - \exp(-\eta), \quad (16)$$

$$\theta_0(\eta) = \exp(-\eta), \quad (17)$$

and the auxiliary linear operators are selected in the following forms:

$$\mathcal{L}_f = \frac{\mathrm{d}^3 f}{\mathrm{d}\eta^3} - \frac{\mathrm{d}f}{\mathrm{d}\eta}, \quad (18)$$

$$\mathcal{L}_\theta = \frac{\mathrm{d}^2 \theta}{\mathrm{d}\eta^2} - \theta. \quad (19)$$

Note that the above operators have the following properties:

$$\mathcal{L}_f[C_1 + C_2\exp(\eta) + C_3\exp(-\eta)] = 0, \quad (20)$$

$$\mathcal{L}_\theta[C_4\exp(\eta) + C_5\exp(-\eta)] = 0, \quad (21)$$

where C_i $(i = 1-5)$ are arbitrary constants.

If $p \in [0,1]$ is an embedding parameter and $\hbar_f$ and $\hbar_\theta$ denote the non-zero auxiliary parameters, respectively, then the zeroth-order deformation problems are constructed as follows:

$$(1-p)\mathcal{L}_f[\hat{f}(\eta,p) - f_0(\eta)] = p\hbar_f \mathcal{N}_f[\hat{f}(\eta,p), \hat{\theta}(\eta,p)], \quad (22)$$

$$(1-p)\mathcal{L}_\theta[\hat{\theta}(\eta,p) - \theta_0(\eta)] = p\hbar_\theta \mathcal{N}_\theta[\hat{f}(\eta,p), \hat{\theta}(\eta,p)], \quad (23)$$

$$\hat{f}(\eta;p)\big|_{\eta=0} = S, \quad \left.\frac{\partial \hat{f}(\eta;p)}{\partial \eta}\right|_{\eta=0} = 1, \quad \left.\frac{\partial \hat{f}(\eta;p)}{\partial \eta}\right|_{\eta=\infty} = 0, \quad (24)$$

$$\hat{\theta}(\eta;p)\big|_{\eta=0} = 1, \quad \hat{\theta}(\eta;p)\big|_{\eta=\infty} = 0, \quad (25)$$

in which the nonlinear operators $\mathcal{N}_f$ and $\mathcal{N}_\theta$ are

$$\begin{aligned}
&\mathcal{N}_f[\hat{f}(\eta;p), \hat{\theta}(\eta;p)] = \\
&\frac{\partial^3 \hat{f}(\eta,p)}{\partial \eta^3} + (1+\lambda_1)\left[\hat{f}(\eta,p)\frac{\partial^2 \hat{f}(\eta,p)}{\partial \eta^2} - \left(\frac{\partial hf\eta}{\partial \eta}\right)^2 - M^2\frac{\partial \hat{f}(\eta,p)}{\partial \eta} - \zeta\left(\frac{\eta}{2}\frac{\partial^2 \hat{f}(\eta,p)}{\partial \eta^2} + \frac{\partial \hat{f}(\eta,p)}{\partial \eta}\right) + \lambda\hat{\theta}(\eta,p)\right] \\
&+ \beta\left[\zeta\left(\frac{\eta}{2}\frac{\partial^4 \hat{f}(\eta,p)}{\partial \eta^4} + 2\frac{\partial \hat{f}^3(\eta,p)}{\partial \eta^3}\right) + 2\frac{\partial \hat{f}(\eta,p)}{\partial \eta}\frac{\partial^3 \hat{f}(\eta,p)}{\partial \eta^3} + 3\left(\frac{\partial^2 \hat{f}(\eta,p)}{\partial \eta^2}\right)^2 - \hat{f}(\eta,p)\frac{\partial^4 \hat{f}(\eta,p)}{\partial \eta^4}\right],
\end{aligned} \quad (26)$$

$$\begin{aligned}
&\mathcal{N}_\theta[\hat{f}(\eta;p), \hat{\theta}(\eta;p)] = \\
&\frac{1}{Pr}\left(1 + \frac{4}{3Nr}\right)\frac{\partial^2 \hat{\theta}(\eta,p)}{\partial \eta^2} + \hat{f}(\eta,p)\frac{\partial \hat{\theta}(\eta,p)}{\partial \eta} - \frac{\partial \hat{f}(\eta;p)}{\partial \eta}\hat{\theta}(\eta;p) \\
&- \frac{\zeta}{2}\left(\eta\frac{\partial \hat{\theta}(\eta,p)}{\partial \eta} + 4\hat{\theta}(\eta,p)\right).
\end{aligned} \quad (27)$$

When $p=0$ and $p=1$, we have

$$\hat{f}(\eta;0)=f_0(\eta),\quad \hat{f}(\eta,1)=f(\eta), \tag{28}$$

$$\hat{\theta}(\eta;0)=\theta_0(\eta),\quad \hat{\theta}(\eta,1)=\theta(\eta), \tag{29}$$

By Taylor's theorem, we obtain

$$\hat{f}(\eta;p)=f_0(\eta)+\sum_{m=1}^{\infty} f_m(\eta)p^m, \tag{30}$$

$$\hat{\theta}(\eta;p)=\theta_0(\eta)+\sum_{m=1}^{\infty} \theta_m(\eta)p^m, \tag{31}$$

$$\begin{aligned} f_m(\eta)&=\frac{1}{m!}\frac{\partial^m f(\eta;p)}{\partial \eta^m}\bigg|_{p=0},\\ \theta_m(\eta)&=\frac{1}{m!}\frac{\partial^m \theta(\eta;p)}{\partial \eta^m}\bigg|_{p=0}. \end{aligned} \tag{32}$$

The auxiliary parameters are so properly chosen that the series (30) and (31) converge at $p=1$, so we have

$$f(\eta)=f_0(\eta)+\sum_{m=1}^{\infty} f_m(\eta), \tag{33}$$

$$\theta(\eta)=\theta_0(\eta)+\sum_{m=1}^{\infty} \theta_m(\eta). \tag{34}$$

The mth-order deformation problems are

$$\mathcal{L}_f[f_m(\eta)-\chi_m f_{m-1}(\eta)]=\hbar_f \mathcal{R}_m^f(\eta), \tag{35}$$

$$\mathcal{L}_\theta[\theta_m(\eta)-\chi_m \theta_{m-1}(\eta)]=\hbar_\theta \mathcal{R}_m^\theta(\eta), \tag{36}$$

$$\begin{aligned} &f_m(0)=0,\quad f_m'(0)=0,\quad f_m'(\infty)=0,\\ &\theta_m(0)=0,\quad \theta_m(\infty)=0, \end{aligned} \tag{37}$$

$$\begin{aligned} \mathcal{R}_m^f(\eta)&=f_{m-1}'''+(1+\lambda_1)\Bigg[-M^2 f_{m-1}'\\ &-\zeta\left(\frac{\eta}{2}f_{m-1}''+f_{m-1}'\right)+\sum_{k=0}^{m-1}\Bigg(f_{m-1-k}f_k''-f_{m-1-k}'f_k'\\ &+\lambda(\theta_{m-1-k}+N\phi_{m-1-k})\Bigg)\Bigg]+\beta\Bigg[\zeta\left(\frac{\eta}{2}f_{m-1}^{iv}+2f_{m-1}'''\right)\\ &+\sum_{k=0}^{m-1}(2f_{m-1-k}'f_k''+3f_{m-1-k}''f_k''-f_{m-1-k}f_k^{iv})\Bigg], \end{aligned} \tag{38}$$

$$\begin{aligned} \mathcal{R}_m^\theta(\eta)&=\frac{1}{Pr}\left(1+\frac{4}{3Nr}\right)\theta_{m-1}''\\ &\quad-\frac{\zeta}{2}(\eta\theta_{m-1}'+4\theta_{m-1})\\ &\quad+\sum_{k=0}^{m-1}[f_{m-1-k}\theta_k'-\theta_{m-1-k}f_k'], \end{aligned} \tag{39}$$

$$\chi_m=\begin{cases}0, & m\le 1,\\ 1, & m>1.\end{cases} \tag{40}$$

The general solutions of (33) and (34) are

$$f_m(\eta)=f_m^*(\eta)+C_1+C_2\exp(\eta)+C_3\exp(-\eta), \tag{41}$$

$$\theta_m(\eta)=\theta_m^*(\eta)+C_4\exp(\eta)+C_5\exp(-\eta), \tag{42}$$

where $f_m^*(\eta)$, $\theta_m^*(\eta)$, and $\phi_m^*(\eta)$ denote the special solutions and

$$\begin{aligned} &C_1=-C_3-f_m^*(0),\quad C_2=C4=0,\\ &C_3=\frac{\partial f_m^*(\eta)}{\partial \eta}\bigg|_{\eta=0},\quad C_5=-\theta_m^*(0). \end{aligned} \tag{43}$$

4. Convergence of the Homotopy Solutions

We note that the solutions (33) and (34) consist of $\hbar_f$ and $\hbar_\theta$ which can adjust and control the convergence of the series solutions. To find the admissible values of $\hbar_f$ and $\hbar_\theta$ of the functions $f''(0)$ and $\theta'(0)$, the $\hbar_f$ and $\hbar_\theta$-curves are displayed for 15th-order of approximations. It is obvious from Figure 1 that the range for the admissible values of $\hbar_f$ and $\hbar_\theta$ are $-0.8\le\hbar_f$ and $\hbar_\theta\le-0.3$. The residual error for the functions f and θ at $\eta=0$ are plotted in Figure 2. Performed computations further show that the series given by (33) and (34) converge in the whole region of η when $\hbar_f=\hbar_\theta=-0.6$.

5. Results and Discussion

This section shows the effects of pertinent parameters on f' and θ. For this purpose, we plotted Figures 3–9. The numerical values of skin friction coefficient $Re_x^{1/2}C_f$ and the local Nusselt number $Re_x^{-1/2}Nu_x$

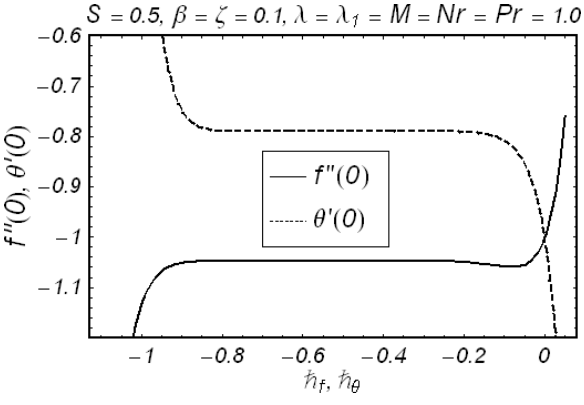

Fig. 1. $\hbar$-curve for the functions f and θ at 15th-order of approximations.

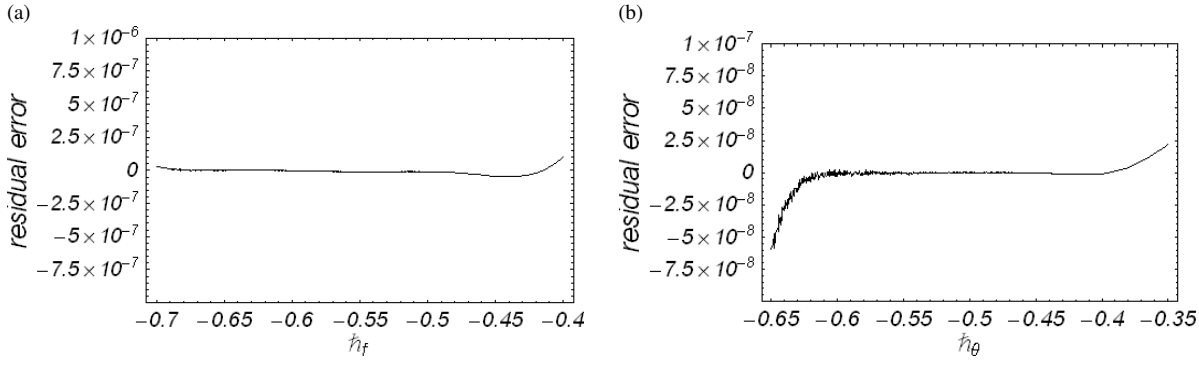

Fig. 2. (a) Residual error for the function f at $\eta = 0$ when $S = 0.5$, $\beta = 0.1$, $\zeta = 0.3$, $\lambda = M = Pr = Nr = 1.0$ (20th-order of app.). (b) Residual error for the function θ at $\eta = 0$ with the same parameters.

Table 1. Values of skin friction coefficient $Re_x^{1/2}C_f$ and local Nusselt number $Re_x^{-1/2}Nu_x$ for some values of S, β, ζ, M, and λ when $Pr = Nr = 1.0$.

S	β	ζ	λ	M	$-Re_x^{1/2}C_f$	$-Re_x^{-1/2}Nu_x$
0.0	0.1	0.1	1.0	1.0	1.041247	0.682991
0.3					1.164567	0.745214
0.5					1.252387	0.790209
0.7					1.343877	0.838091
	0.0				1.241597	0.820287
	0.2				1.464787	0.851097
	0.3				1.585177	0.868517
	0.4				1.701427	0.870253
	0.1	0.0			1.289837	0.779392
		0.2			1.359127	0.892452
		0.4			1.490937	0.990791
		0.6			1.580127	0.078577
		0.1	0.5		1.582697	0.807630
			0.8		1.437437	0.826797
			1.2		1.252477	0.848474
			1.5		1.118890	0.862683
			1.0	0.5	1.008717	0.873676
				0.8	1.192077	0.853977
				1.0	1.343877	0.838090
				1.2	1.511647	0.821081

Table 2. Values of skin friction coefficient $Re_x^{1/2}C_f$ and local Nusselt number $Re_x^{-1/2}Nu_x$ for some values of Pr and Nr when $S = 0.7$, $\zeta = 0.1$, and $\lambda = M = 1.0$.

Pr	Nr	$-Re_x^{1/2}C_f$	$-Re_x^{-1/2}Nu_x$
0.8	1.0	1.306197	0.722779
1.2		1.375857	0.947961
1.5		1.416037	1.105217
2.0		1.468527	1.352727
	0.8	1.444157	1.230907
	1.2	1.486697	1.452777
	1.5	1.506077	1.573617
	2.0	1.528867	1.722897

for various values of emerging parameters are given in Tables 1 and 2. Figure 3 displays the effects of suction parameter S on the velocity and temperature profiles. Velocity and temperature are found to decrease with the increasing values of S. This follows from the fact that the heated fluid is pushed towards the wall, where the buoyancy forces can act to retard the fluid due to the high influence of viscosity. This effect acts to decrease the wall shear stress. The boundary layer thickness for temperature reduces in case of suction. The effect of Deborah number is explained in Figure 4. It is seen that the velocity and the boundary layer thickness are increasing functions of the Deborah number. However, the temperature profile decreases upon increasing Deborah number β. The influence of unsteadiness parameter on the fluid velocity and temperature is discussed in Figure 5. Appreciable change for the rate of increase in velocity and temperature is observed. The influence of mixed convection parameter λ is shown in Figure 6. The increasing values of λ indicate the larger temperature and concentration gradient from the wall relative to the ambient. In other words, the increasing values of λ corresponds to the stronger buoyancy force and thus lead to the larger velocity. The larger velocity accompanies with the decreasing boundary layer thickness for temperature. The effect of Hartman number is explained in Figure 7. It is obvious that the application of magnetic field causes higher restriction to the fluid, which reduces the fluid velocity (Fig. 7a) and enhanced the temperature. The effect of Prandtl number Pr on the velocity and temperature fields is plotted in Figure 8. The boundary layer thickness decreases by increasing Prandtl number for the temperature field. From the physical point of view, the higher Prandtl number coincides with the weaker thermal diffusivity and thinner thermal boundary layer thickness.

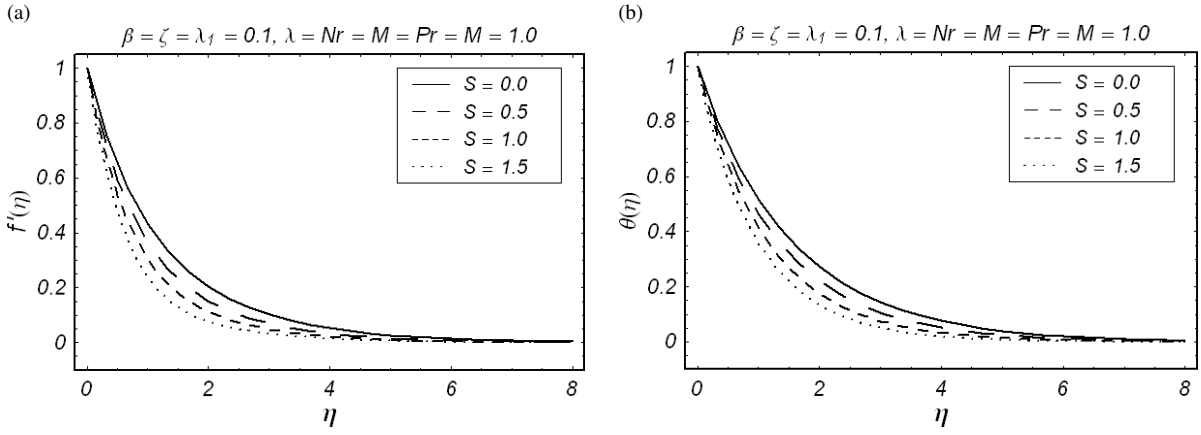

Fig. 3. Effect of suction parameter S on f' and θ.

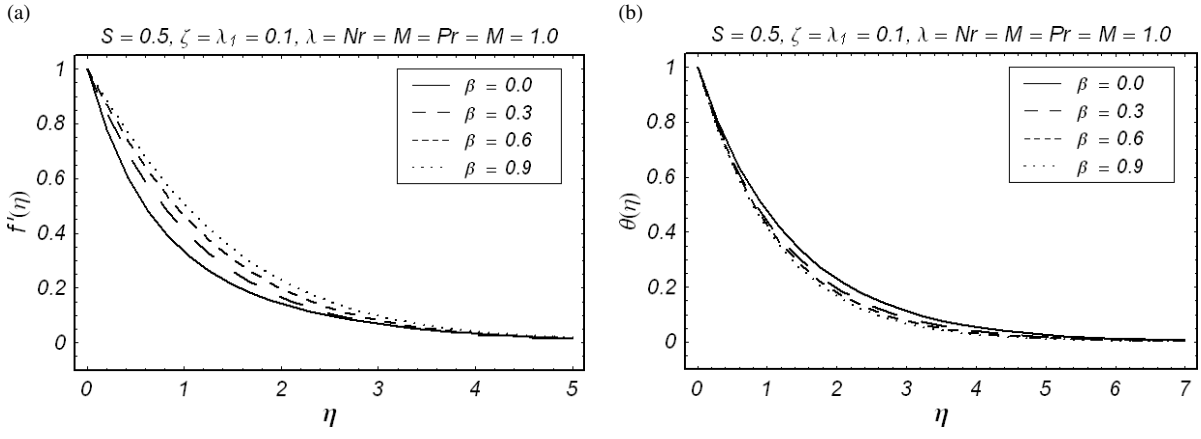

Fig. 4. Effect of Deborah number β on f' and θ.

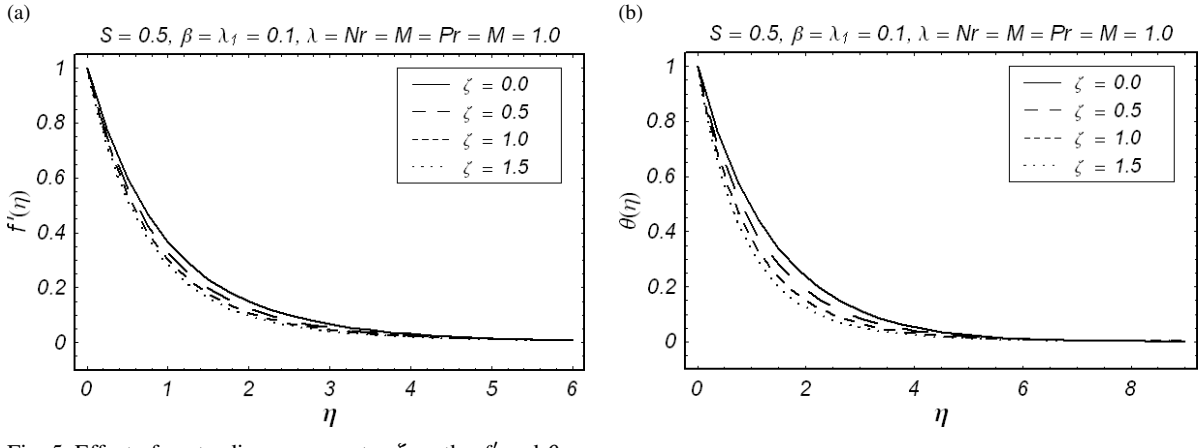

Fig. 5. Effect of unsteadiness parameter ζ on the f' and θ.

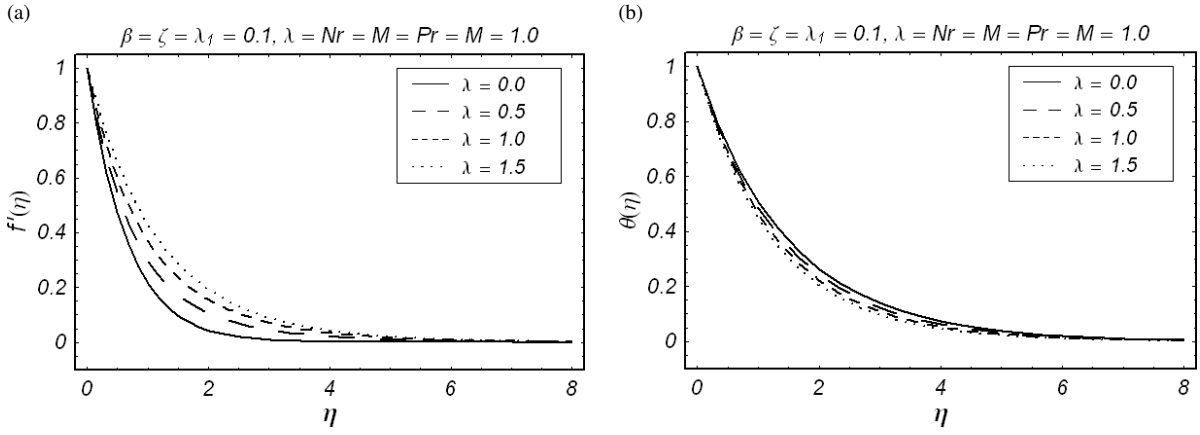

Fig. 6. Effect of mixed convection parameter λ on f' and θ.

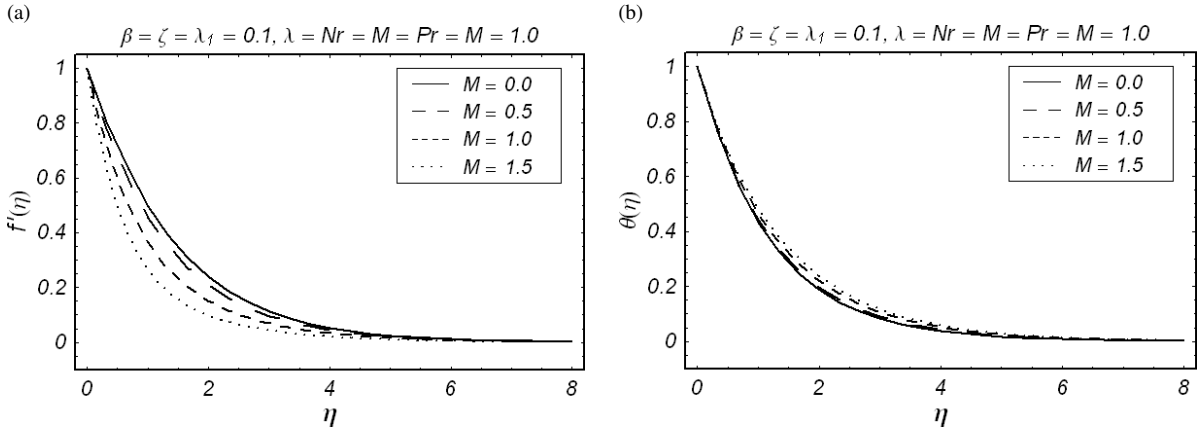

Fig. 7. Effect of Hartman number M on f' and θ.

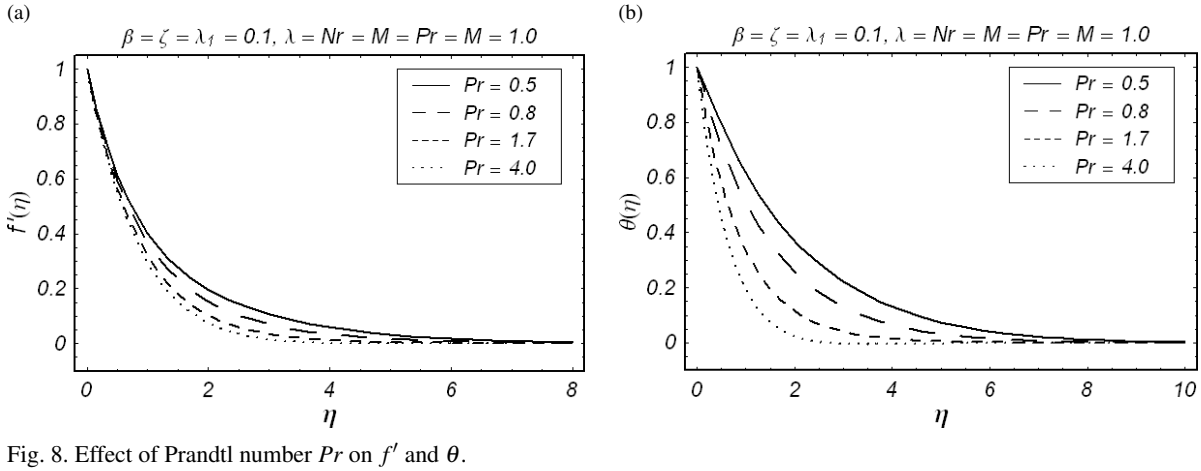

Fig. 8. Effect of Prandtl number Pr on f' and θ.

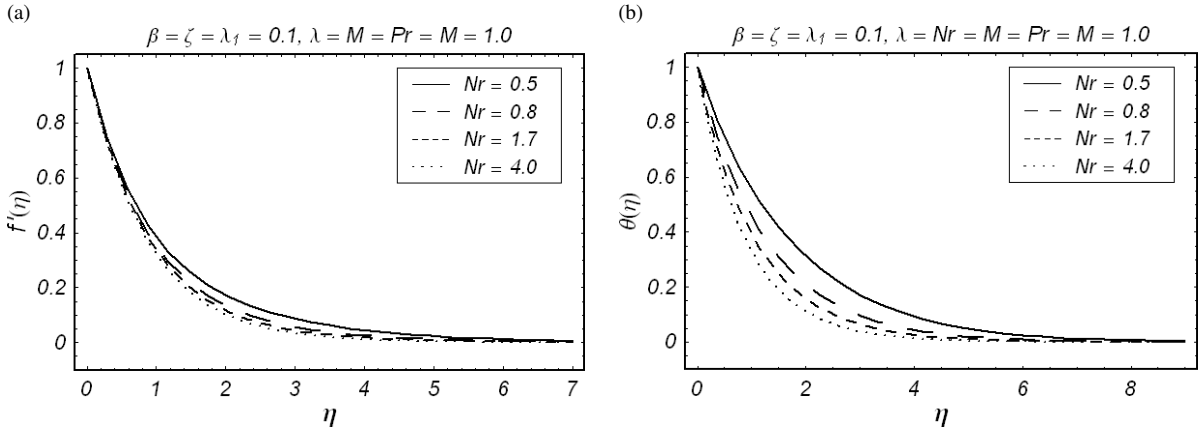

Fig. 9. Effect of radiation parameter Nr on f' and θ.

The influence of radiation parameter Nr on the velocity and temperature profiles is discussed in Figure 9. This figure depict that both, the velocity and temperature fields, decrease for large values of Nr.

Tables 1 and 2 show the values of the skin friction coefficient $Re_x^{1/2}C_f$ and the local Nusselt number $Re_x^{-1/2}Nu_x$. The magnitude of the skin friction coefficient increases with the increase of S, β, ζ, m, and Pr. However, it decreases with the increase in λ. The magnitude of the local Nusselt number increases for large values of S, ζ, Pr, and Nr. There is a decrease in the local Nusselt number for large values of β, λ, and M.

[1] C. Fetecau and C. Fetecau, Int. J. Eng. Sci. **43**, 781 (2005).
[2] C. Fetecau, M. Athar, and C. Fetecau, Comput. Math. Appl. **57**, 596 (2009).
[3] C. Fetecau and C. Fetecau, Int. J. Eng. Sci. **44**, 788 (2006).
[4] W. C. Tan, P. W. Xiao, and X. M. Yu, Int. J. Nonlinear Mech. **38**, 645 (2003).
[5] Kh. S. Mekheimer and Y. Abd Elmaboud, Physica A **387**, 2403 (2008).
[6] M. H. Haroun, Commun. Nonlinear Sci. Numer. Simul. **12**, 1464 (2007).
[7] T. Hayat, Z. Abbas, and M. Sajid, Phys. Lett. A **372**, 2400 (2008).
[8] Z. Abbas, Y. Wang, T. Hayat, and M. Oberlack, Int. J. Nonlinear Mech. **43**, 783 (2008).
[9] T. Hayat, M. Sajid, and M. Ayub, Commun. Nonlinear Sci. Numer. Simul. **13**, 745 (2008).
[10] T. Hayat, M. A. Farooq, T. Javed, and M. Sajid, Nonlinear Anal. : Real World Applications **10**, 745 (2009).
[11] L. J. Crane, Z. Angew. Math. Phys. **21**, 645 (1970).
[12] S. J. Liao, Fluid Mech. **488**, 189 (2003).
[13] Z. Abbas and T. Hayat, Int. J. Heat Mass Transfer **51**, 1024 (2008).
[14] R. Cortell, Int. J. Nonlinear Mech. **41**, 78 (2006).
[15] M. Sajid and T. Hayat, Int. Commun. Heat Mass Transfer **35**, 347 (2008).
[16] P. D. Ariel, T. Hayat, and S. Ashgar, Acta Mech. **187**, 29 (2006).
[17] A. Ishak, R. Nazar, and I. Pop, Heat Mass Transfer **44**, 921 (2008).
[18] T. Hayat, Z. Abbas, and M. Sajid, Theor. Comput. Fluid Dyn. **20**, 229 (2006).
[19] R. Cortell, Phys. Lett A **372**, 631 (2008).
[20] S. J. Liao, Int. J. Heat Mass Transfer **48**, 2529 (2008).
[21] C. D. S. Devi, H. S. Takhar, and G. Nath, Heat Mass Transfer **26**, 71 (1991).
[22] H. I. Andersson, J. B. Aarseth, and B. S. Dandapat, Int. J. Heat Mass Transfer **43**, 69 (2003).
[23] R. Nazar, N. Amin, and I. Pop, Mech. Res. Commun. **31**, 121 (2004).
[24] E. M. A. Elbashbeshy and M. A. A. Bazid, Heat Mass Transfer **41**, 1 (2004).
[25] S. Mukhopadhyay, Int. J. Heat Mass Transfer **52**, 3261 (2009).
[26] J. E. Daskalakis, Can. J. Phys. **70**, 1253 (1993).
[27] M. Ali and F. Al-Yousef, Heat Mass Transfer **33**, 301 (1998).
[28] C. H. Chen, Heat Mass Transfer **33**, 471 (1998).
[29] C. H. Chen, Heat Mass Transfer **36**, 79 (2000).
[30] M. Ali, Heat Mass Transfer **40**, 285 (2004).
[31] S. J. Liao, Commun. Nonlinear Sci. Numer. Simul. **14**, 2144 (2009).

[32] H. Xu, S. J. Liao, and X. C. You, Commun. Nonlinear Sci. Numer. Simul. **14**, 1152 (2009).
[33] H. Xu and S. J. Liao, Commun. Nonlinear Sci. Numer. Simul. **13**, 350 (2008).
[34] S. J. Liao, Appl. Math. Comput. **169**, 1186 (2005).
[35] Y. Tan and S. Abbasbandy, Commun. Nonlinear Sci. Numer. Simul. **13**, 539 (2008).
[36] S. Abbasbandy, Phys. Lett. A **372**, 613 (2008).
[37] S. Abbasbandy and F. S. Zakaria, Nonlinear Dyn. **51**, 83 (2008).
[38] S. Kechil and I. Hashim, Commun. Nonlinear Sci. Numer. Simul. **14**, 1346 (2009).
[39] I. Hashim, O. Abdulaziz, and S. Momani, Commun. Nonlinear Sci. Numer. Simul. **14**, 674 (2009).
[40] M. Sajid, T. Hayat, and S. Asghar, Int. J. Heat Mass Transfer **50**, 1723 (2007).
[41] T. Hayat and Z. Abbas, Chaos, Soliton, and Fractals **38**, 556 (2008).
[42] M. Sajid, I. Ahmed, T. Hayat, and M. Ayub, Commun. Nonlinear Sci. Numer. Simul. **13**, 2193 (2008).
[43] T. Hayat, T. Javed, and M. Sajid, Phys. Lett. A **372**, 3264 (2008).
[44] M. Sajid and T. Hayat, Int. Commun. Heat Mass Transfer **36**, 59 (2009).
[45] M. Sajid and T. Hayat, Chaos, Soliton, and Fractals **38**, 506 (2008).